

Dumbbell Dual-Hairpin Triggered DNA Nanonet Assembly for Cascade-Amplified Sensing of Exosomal MicroRNA

Yongxing Li,^{||} Xiaoqi Tang,^{||} Ruijia Deng, Liu Feng, Shuang Xie, Ming Chen,^{*} Ji Zheng,^{*} and Kai Chang^{*}



Cite This: *ACS Omega* 2024, 9, 19723–19731



Read Online

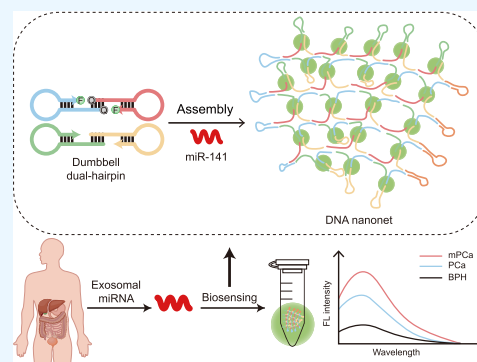
ACCESS |

Metrics & More

Article Recommendations

Supporting Information

ABSTRACT: Exosomal microRNAs (miRNAs) are valuable biomarkers closely associated with cancer progression. Therefore, sensitive and specific exosomal miRNA biosensing has been employed for cancer diagnosis, prognosis, and prediction. In this study, a miRNA-based DNA nanonet assembly strategy is proposed, enabling the biosensing of exosomal miRNAs through dumbbell dual-hairpin under isothermal enzyme-free conditions. This strategy dexterously designs a specific dumbbell dual-hairpin that can selectively recognize exosomal miRNA, inducing conformational changes to cascade-generated X-shaped DNA structures, facilitating the extension of the X-shaped DNA in three-dimensional space, ultimately forming a DNA nanonet assembly. On the basis of the target miRNA, our design enriches the fluorescence signal through the cascade assembly of DNA nanonet and realizes the secondary signal amplification. Using exosomal miR-141 as the target, the resultant fluorescence sensing demonstrates an impressive detection limit of 57.6 pM and could identify miRNA sequences with single-base variants with high specificity. Through the analysis of plasma and urine samples, this method effectively distinguishes between benign prostatic hyperplasia, prostate cancer, and metastatic prostate cancer. Serving as a novel noninvasive and accurate screening and diagnostic tool for prostate cancer, this dumbbell dual-hairpin triggered DNA nanonet assembly strategy is promising for clinical applications.



INTRODUCTION

Exosomes have emerged as a promising target for liquid biopsy, thanks to their abundance in body fluids, stable circulation, and specific bioactive cargo.^{1–4} Of particular interest are microRNAs (miRNAs) found within exosomes, which are derived from donor cells and act on recipient cells as essential gene expression regulators,^{5–7} mediating intercellular communication and influencing cancer development.^{8–11} MiRNAs within exosomes have demonstrated superior sensitivity and specificity compared to single cancer protein markers, making them valuable tools for early cancer screening, predicting cancer tumor, node, metastasis (TNM) staging, assessing prognosis, monitoring therapeutic effects, and evaluating drug resistance.^{12–15} Therefore, the detection of exosomal miRNAs offers the potential for accurate and noninvasive diagnosis of patients, aligning with the trend of precision medicine and holding promising prospects for widespread clinical applications.^{16–19}

Emerging DNA-based nanotechnologies, such as strand displacement amplification, catalytic hairpin assembly, and rolling circle amplification, hybrid chain reaction (HCR), capitalize on DNA's Watson–Crick base pairing and programmable sequences,^{20–22} serving as viable solutions for nucleic acid, infectious microorganisms, and toxic metal ions biosensing.^{23–27} Among these, HCR stands out for its exceptional sensitivity and specificity. Additionally, its enzyme-free and

constant temperature attributes simplify instrument usage and reduce experimental costs,^{28–31} thus enhancing its relevance in biosensor development. Dirks et al. proposed the classical HCR system, utilizing complementary DNA hairpins and initiators with sticky ends to generate simple one-dimensional DNA nanostructures for signal amplification.³² However, the sensitivity of this traditional HCR system was suboptimal, and the reaction kinetics were limited.²⁸ Hence, two-dimensional DNA biosensing systems, such as multibranch HCR^{33–36} and net-like HCR,^{37,38} have achieved exponential signal amplification of DNA structures in a two-dimensional space through DNA nanoassembly, building upon Dirks et al.'s linear signal amplification foundation. The dumbbell hairpin is a specially designed probe that has been widely applied in liquid biopsy.^{39–42} Chen et al. designed a dumbbell hairpin that can recognize dual miRNAs simultaneously, combined Ag⁺ and Hg²⁺, and used CdTe quantum dots and carbon dots to achieve signal amplification for enzyme-free amplification and instant

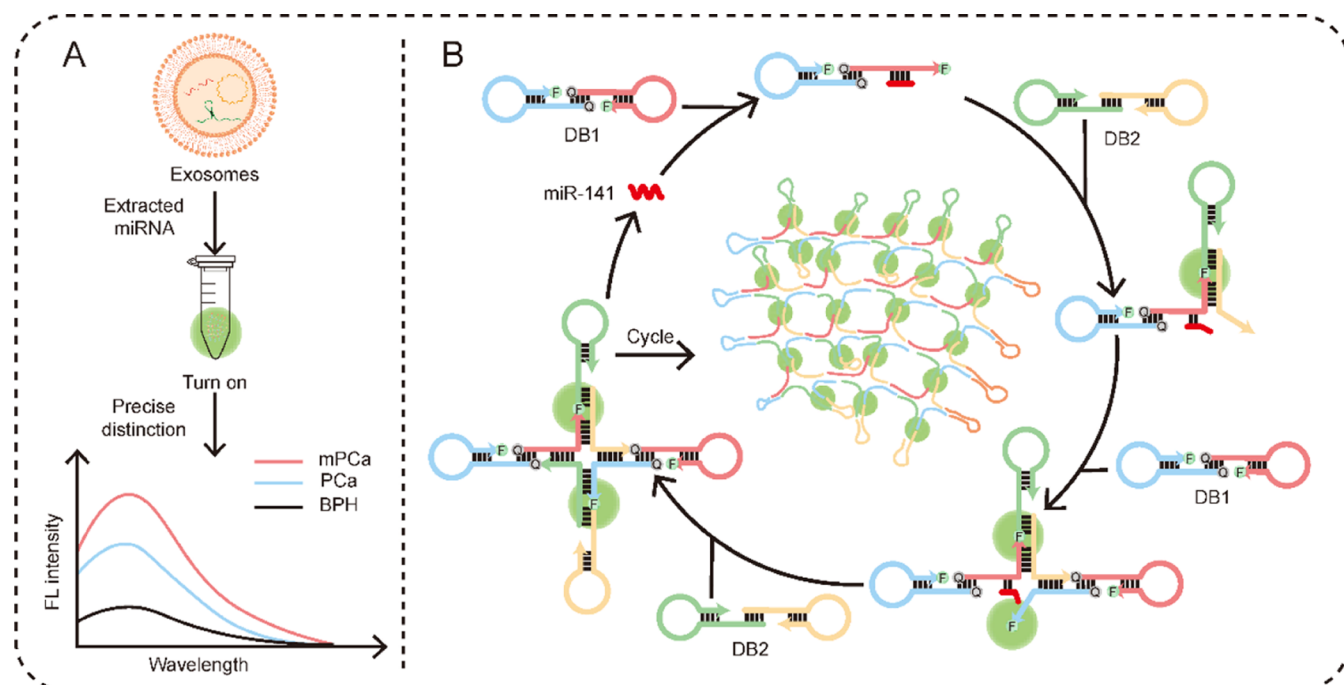
Received: March 18, 2024

Revised: April 7, 2024

Accepted: April 10, 2024

Published: April 22, 2024



Scheme 1. Illustration of Our Strategy^a

^a(A) The process of our method implementation. (B) Dumbbell dual-hairpin triggered DNA nanonet assembly for cascade-amplified sensing of exosomal microRNA.

detection of dual miRNAs in urine.⁴³ Dong et al. developed a dumbbell probe based on entropy-driven strand displacement reaction, capable of specifically identifying the altered fluorescence (FL) signal produced by miR-193b and A β 42 oligomers, and used graphene oxide to reduce the background signal for more sensitive detection.⁴⁴ However, these researchers introduced other methods or materials to amplify the sensing signal, treating the dumbbell hairpin as a simple tool for signal conversion rather than the main role of signal amplification. Therefore, the application of dumbbell hairpins in biosensing is still relatively simple, and there is still a lot of room for play.

Building upon the two-dimensional HCR and programmable DNA sequences, we cleverly designed dumbbell dual-hairpin and constructed the dumbbell dual-hairpin triggered DNA nanonet assembly for cascade-amplified sensing of exosomal miRNA (Scheme 1). Our approach involves the design of two dumbbell dual-hairpins, namely, DB1 and DB2, each comprising H1 and H3, and H2 and H4, respectively. Both sticky ends of H1 and H3 have been modified with FAM and BHQ1, respectively, and the fluorescence signal of FAM was quenched by BHQ1 due to Förster resonance energy transfer (FRET) in the stable state. Upon the presence of specific exosomal miRNA, DB1 and DB2 dumbbells undergo chain substitution, resulting in the formation of an X-shaped DNA structure. The strategic design of the dumbbell dual-hairpin facilitates the extension of the X-shaped DNA in three-dimensional space, promoting further assembly into DNA nanonet. This structural change effectively increases the distance between FAM and BHQ1, inhibiting FRET and enabling the quantification of exosomal miRNA levels. Herein, leveraging the biomarker role of miR-141^{45,46} and its significant expression discrepancies in exosomes among patients with benign prostatic hyperplasia (BPH), prostate cancer (PCa),⁴⁷ and metastatic prostate cancer (mPCa), we established a biosensing model targeting exosomal miR-141. This model enabled the enzyme-free *in vitro* biosensing of exosomal miR-

141, showcasing its immense potential as a precise and noninvasive screening and diagnostic tool for PCa.

EXPERIMENTAL SECTION

Materials and Reagents. All oligonucleotides (Table S1) were synthesized by Sangon Biotechnology (Shanghai, China) and purified using high-performance liquid chromatography (HPLC). Sodium chloride was obtained from Sigma-Aldrich. Magnesium chloride hexahydrate was purchased from Solarbio Science & Technology Co., Ltd. (Beijing, China). Sodium 4-(2-hydroxyethyl)-1-piperazineethanesulfonic acid (HEPES) was procured from Sangon Biotechnology Co., Ltd. (Shanghai, China). Sodium dodecyl sulfate-polyacrylamide gel electrophoresis (SDS-PAGE) gel preparation reagents were acquired from Beyotime Biotechnology (Shanghai, China). 5 \times Tris/borate/EDTA (TBE) buffer was sourced from Solarbio Life Sciences (Beijing, China). The 20 bp DNA ladder was obtained from Takara Bio (Shiga, Japan). Super GelRed nucleic acid stain was supplied by Biotium (Fremont, USA). The buffer used in this study was a mixed HEPES buffer composed of 10 mM HEPES, 1 M NaCl, and 50 mM MgCl₂, adjusted to pH 7.4.⁴⁸ A stock solution of oligonucleotides was prepared by dissolving them in sterile HEPES buffer (10 mM HEPES, 1 M NaCl, and 50 mM MgCl₂) at pH 7.4. All solutions were prepared using ultrapure water (resistivity of 18.2 M Ω /cm) from the Millipore ultrapure water system. Human plasma and urine samples were collected from Southwest Hospital, Chongqing, China. The patient sample experiment was approved by the Ethics Committee of the First Affiliated Hospital of the Army Medical University (KY201993).

Detection Procedure. Four hairpin DNAs (H1, H2, H3, H4) were denatured at 95 °C for 5 min, followed by annealing at 25 °C for 2 h to achieve the designed hairpin structures. In 20 μ L of hybridization buffer (10 mM HEPES, 1 M NaCl, 50 mM

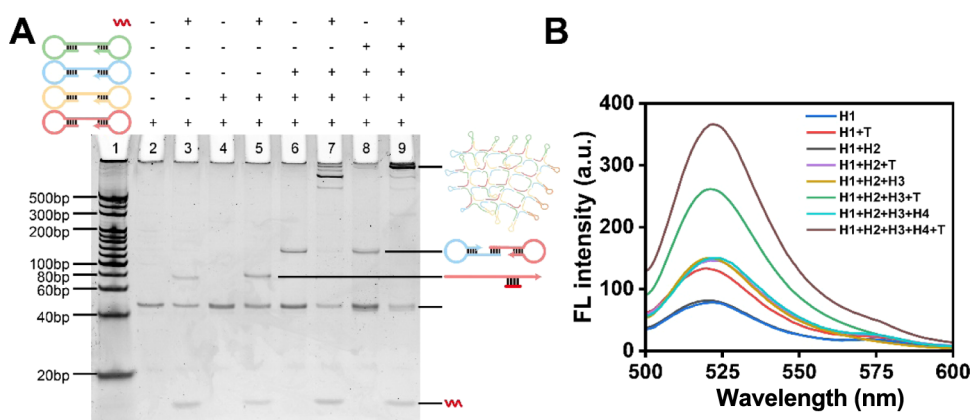


Figure 1. Verification of our design. (A) Polyacrylamide gel electrophoresis analysis. Lane 1: 20 bp DNA ladder; lane 2: H1; lane 3: T + H1; lane 4: H1 + H2; lane 5: T + H1 + H2; lane 6: H1 + H2 + H3; lane 7: T + H1 + H2 + H3; lane 8: H1 + H2 + H3 + H4; lane 9: T + H1 + H2 + H3 + H4. (B) Fluorescence spectra in the presence and absence of T. Concentrations: miR-141, 10 nM; H1, H2, H3, H4, 100 nM.

MgCl₂, pH 7.4), concentrations of 100 nM of H1, H2, H3, and H4 were present. Various concentrations of miR-141 were added to catalyze the assembly reaction. After incubating at 40 °C for 3 h, the mixture underwent structural characterization and fluorescence measurements at least three times. Fluorescence spectra were recorded by using an F-7000 fluorescence spectrophotometer. The excitation wavelength was set at 480 nm, and fluorescence data were collected within the range of 500–600 nm.

Characterizations. The size and morphology of the DNA nanonet assembly were measured with a Bruker Dimension Icon atomic force microscope (Bruker, Germany). Nanoparticle tracking analysis (NTA) was performed using a Zetasizer Nano ZS90 (Malvern Instrument Ltd., U.K.). Fluorescence spectra were performed with an F-7000 fluorescence spectrophotometer (Hitachi Co. Ltd., Japan). The reverse transcription quantitative polymerase chain reaction (qRT-qPCR) analysis was recorded with a CFX96 real-time system (Bio-Rad).

12% PAGE Gel Electrophoresis. Target miRNA was combined with dumbbell dual-hairpin and incubated at 40 °C for 3 h (each hairpin probe concentration was maintained at 100 nM). After the reaction, 5 μ L of each reaction product was mixed with 1 μ L of a 6 \times loading buffer and subjected to 12% PAGE gel electrophoresis. The gel was run at a constant voltage of 130 V in 1 \times Tris/borate/EDTA (TBE) buffer for 50 min, visualized under UV light, and gel images were captured using a digital camera.

Atomic Force Microscopy (AFM). A 200 μ L aliquot of the prepared sample was deposited onto a mica sheet, allowed to air-dry, and subsequently imaged using Bruker Dimension Icon AFM.

Exosome Isolation. Plasma and urine samples were collected from patients and subjected to centrifugation at 3000 *g* for 20 min at room temperature. The supernatant was collected and further centrifuged at 10 000 *g* for 30 min at room temperature. The supernatant was prefiltered using a 0.22 μ m filter. Subsequently, exosome extraction was performed using the exoEasy Maxi Kit (Qiagen, Hilden, Germany) according to the manufacturer's instructions.

Transmission Electron Microscopy (TEM). The sealing film was carefully positioned on the glass sheet, and the copper mesh was delicately placed onto the sealing film by using tweezers. A 10 μ L aliquot of exosomes was applied to the copper mesh. Following a 10 min of incubation, the surplus liquid was

absorbed using a small piece of filter paper, and subsequently, a 10 μ L volume of 3% uranyl acetate was applied to the copper mesh. The sample was air-dried before imaging with an FEI Tecnai G2 12 transmission electron microscope (FEI).

Western Blotting. The cellular or exosomal total proteins were obtained from radioimmunoprecipitation assay (RIPA) lysates and quantified using a bicinchoninic acid (BCA) protein assay kit. Subsequently, the total proteins were separated via SDS-PAGE gel and transferred to a polyvinylidene fluoride (PVDF) membrane (Millipore). Following a 1 h blocking step in 5% skim milk, the membrane was probed with CD63 antibody (1:1000), CD81 antibody (1:500), and GAPDH antibody (1:10 000), overnight at 4 °C. This was followed by incubation with secondary antibody at 37 °C for 2 h. Imaging was achieved using an enhanced chemiluminescence (ECL) reagent (Beyotime, China).

Extraction and qRT-PCR Analysis of Exosomal miRNAs. Total RNA from exosomes in plasma and urine was extracted using the exoRNeasy Midi Kit (Qiagen) following the manufacturer's instructions and previous studies.⁴⁷ Total microRNA was reverse-transcribed into cDNA using the miScript II RT Kit (Qiagen) following the manufacturer's protocol. After the template miRNA was added, the reverse transcription enzyme was inactivated by heating at 85 °C for 5 min. Subsequently, qRT-PCR was conducted at least three times, using the miScript SYBR Green PCR Kit (Qiagen), with cycling conditions set at 95 °C for 5 s followed by 40 cycles of 60 °C for 20 s.

RESULTS AND DISCUSSION

Construction of Dumbbell Dual-Hairpin-Triggered DNA Nanonet Assembly. This paper introduces a novel biosensing approach for precise PCa diagnosis, employing exosomal miR-141 and dumbbell dual-hairpin. The biosensing system comprises two dumbbell dual-hairpins, DB1 and DB2, consisting of H1 and H3, H2 and H4, respectively. H1, H2, H3, and H4 are designed to complement themselves with 16 and 6 bases at the 5' end and 3' end, respectively, and could stably form dumbbell hairpins without other interference. The close distance between FAM and BHQ1 quenches the fluorescence signal of FAM. Moreover, there is a long complementary sequence of 20 bases between H1 and H3, and H2 and H4, allowing the form of a dumbbell dual-hairpin and the quench of FAM. In the presence of specific exosomal miRNA (T), T can

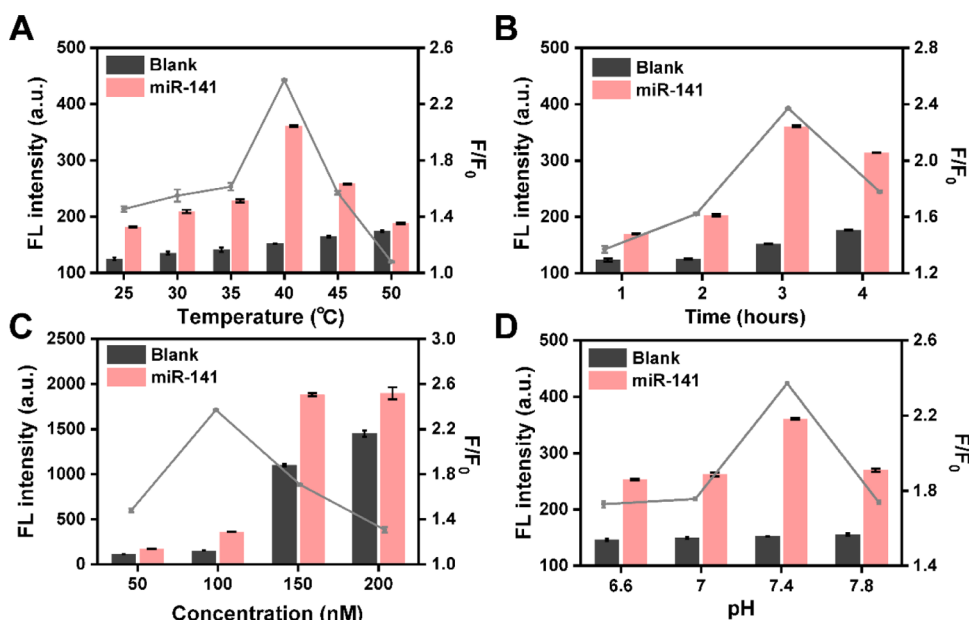


Figure 2. Optimization of important experimental factors. (A) Temperature optimization. (B) Time optimization. (C) Hairpin concentration. (D) pH optimization. Concentrations: miR-141, 10 nM; H1, H2, H3, H4, 100 nM. F and F_0 represent the fluorescence intensities of the probes in the presence and absence of miR-141, respectively.

act on H1 in DB1 and undergo a chain substitution reaction with DB1, leading to the exposure of the 3' end in H1. The 3' end of H1 has specific complementary capabilities with H2 in DB2, resulting in the structure change in H2. H3 and H4 undergo hairpin structure changes to form X-shaped DNA, and T is released for the next signal amplification cycle. Based on a single dumbbell hairpin, the dumbbell dual-hairpin has a hairpin that has not been opened at the other end and can activate the next reconstruction triggered by T so that the X-shaped DNA can continue to extend in three-dimensional space, forming a DNA nanonet. In this process, the distance between FAM and BHQ1 increased due to the formation of the DNA nanonet, and the fluorescence signal of FAM was no longer quenched by BHQ1. Furthermore, the formation of DNA nanonet enriched FAM scattered in the solution, and the fluorescence signal was amplified again. Conversely, in the absence of T, the dumbbell dual-hairpin remained in a stable structure, resulting in FRET-induced fluorescence quenching from FAM to BHQ1. Therefore, through the continuous circulation of T and the formation of a DNA nanonet, the signal conversion and secondary amplification from T to FAM are achieved.

To ensure that each hairpin probe undergoes subsequent steps and that the proper construction of the dumbbell dual-hairpin triggered DNA nanonet assembly occurs as described in Scheme 1, gel electrophoresis was performed. As shown in Figure 1A, a comparison with the H1 control (lane 2) revealed that the mixture of H1 and T exhibited partial retardation of electrophoretic mobility (lane 3), indicating the activation of the assembly process by T. Moreover, evident retardation of electrophoretic mobility was observed in lanes 5, 7, and 9, compared to lanes 4, 6, and 8, respectively, further confirming the successful assembly in the presence of T. The concentrated electrophoretic band in lane 9 verified the successful construction of DNA nanonet assembly, which was further supported by fluorescence spectra change (Figure 1B) and atomic force microscopy (AFM) (Figure S1). Upon the presence of the target, the dumbbell dual-hairpin underwent

conformational changes, giving rise to an X-shaped DNA. Consequently, a cyclic reaction was initiated in both horizontal and vertical directions, facilitating mutual complementation and extension in three-dimensional space, thus creating a local DNA nanonet. At the same time, this local DNA nanonet maintains the capability for base complementarity pairing and extension, resulting in the formation of a larger DNA nanonet.

Optimization of Reaction Conditions. To optimize this strategy, we focused on the reaction temperature, assembly time, hairpin concentration, and pH of the buffer. These factors play vital roles in DNA hybridization and the stability of hairpin structures, thereby influencing the signal-to-background (F/F_0) ratio, where F represents the fluorescence intensity of the probes in the presence of miR-141 and F_0 represents the fluorescence intensity in its absence.

After rigorous experimentation, we found that the optimal temperature for our strategy was 40 °C (Figure 2A). At this temperature, we observed a higher F/F_0 ratio due to reduced hairpin stability, making it ideal for subsequent experiments. Furthermore, we monitored the hairpin self-assembly process to form a DNA nanonet assembly at different time intervals (Figure 2B). The F/F_0 ratio increased steadily with assembly time, reaching a peak at approximately 3 h. In contrast, a negligible fluorescence increase was observed in the absence of the target miR-141. As a result, we determined 3 h as the optimal assembly time for future experiments. During the optimization of the reaction temperature and time, we noticed an interesting observation. The FL intensity decreased after reaching a peak in the presence of T. This suggested the possibility of a steric hindrance effect in the DNA nanonet assembly, causing FAM to be closer to BHQ1 than that in a planar configuration. Additionally, we optimized the concentration of the hairpin probes. Based on our findings, the F/F_0 ratio reached its maximum at a hairpin concentration of 100 nM, indicating that 100 nM is the optimal concentration for accurate detection (Figure 2C). Moreover, the pH of the reaction environment was found to be crucial. At pH 7.4, the DNA nanonet assembly

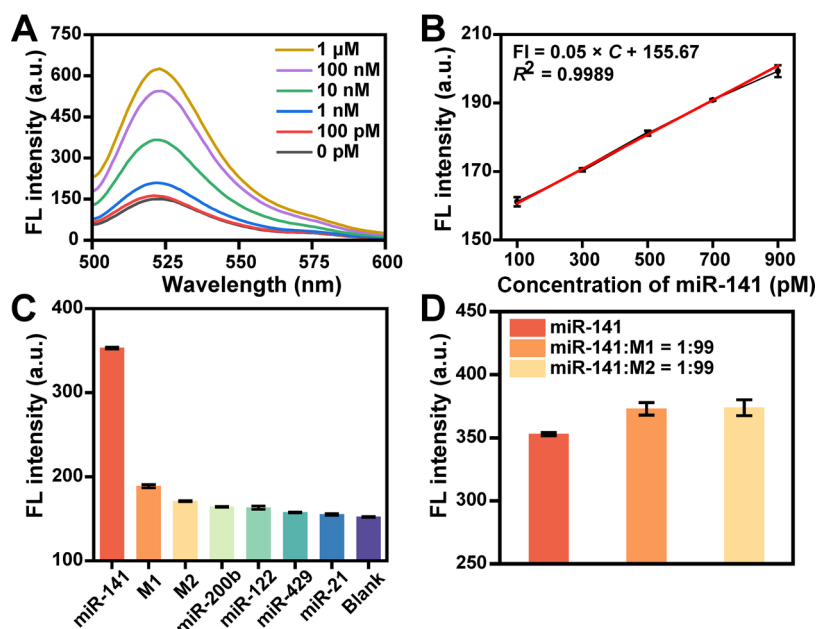


Figure 3. Analytical performance of the experimental design. (A) Fluorescence spectra of various miR-141 concentrations. (B) The linear relationship between the FL intensity and the concentration of miR-141. (C) Specificity of our design for detection of different miRNA species. (D) Identification capacity of our method to detect miR-141 in a miRNA mixture. Concentrations: miR-141, 0 pM to 1 μ M; H1, H2, H3, H4, 100 nM.

activated by T showed optimal effectiveness (Figure 2D). Taking all of these factors into account, we established the optimal reaction conditions: a hairpin concentration of 100 nM, pH 7.4, and a reaction time of 3 h at 40 $^{\circ}$ C.

Sensitivity and Selectivity of miRNA-141 Detection.

To validate the effectiveness of our miR-141 detection strategy, we performed repeated fluorescence spectroscopy under optimal reaction conditions using different concentrations of miR-141, and part of the results are shown in Figure S2. As illustrated in Figure 3A, the fluorescence intensities of the probes showed a gradual increase in proportion to the concentrations of miR-141, demonstrating a linear relationship between miR-141 concentrations of 100 and 900 pM (Figure 3B). The obtained linear regression equation (C , pM) was FL intensity (FI) = $0.05 \times C + 155.67$, with a high correlation coefficient ($R^2 = 0.9989$) and a detection limit of 57.6 pM ($3\sigma/k$). Compared with other isothermal enzyme-free detection methods, the detection limit achieved in this study was higher. Even in the presence of enzymes or precious metal nanomaterials, the decline in detection ability was not obvious, indicating the sensitivity and ingenuity of this study (Table 1).

Concurrently, we assessed the selectivity of our strategy by testing six different oligonucleotides: one with a one-base mismatch (M1), one with a two-base mismatch (M2), miR-200b, miR-122, miR-429, and miR-21. Figure 3C shows that the fluorescence intensity was significantly lower for these oligonucleotides compared to miR-141, even in the presence of a single-base mismatch. In addition, we tested the ability to detect the target in complex mixtures. Figure 3D demonstrates the capability of our proposed strategy to specifically detect the target miR-141 even in complex biological mixtures (miR-141/M1 = 1:99 or miR-141/M2 = 1:99).

Exosomes Characterization. Figure 4A presents the workflow for utilizing exosomal miRNAs in our study. The morphology of the purified exosomes derived from the plasma and urine of patients with BPH, PCa, and mPCa was examined by using TEM. As shown in Figure 4B, the exosomes displayed a

Table 1. Comparison to Other Methods

study materials	targets	linear interval (pM)	limit of detection (pM)	reference
FAM, dumbbell dual-hairpin	miR-141	$10^2 - (9 \times 10^2)$	57.6	our study
FAM, metal-organic framework, T4 DNA ligase, phi29 DNA polymerase	miR-224	$10^3 - (2 \times 10^4)$	200	Sun et al. ⁴⁹
FAM, MnO ₂ nanosheet	miR-21	$10^2 - (2 \times 10^4)$	73	Wang et al. ⁵⁰
AgNCs	miR-21	$10^2 - (2.5 \times 10^4)$	20	Pan et al. ⁵¹
FAM, CDs, T7 exonuclease	miR-21	$50 - 10^4$	1	Wang et al. ⁵²

characteristic saucer-like shape and were stained using uranyl acetate. Additionally, to validate the presence of the surface protein markers CD63 and CD81 on the exosomes, a Western blotting analysis was performed. Figure 4C illustrates distinct bands confirming the presence of CD63 and CD81, further supporting the identification of the isolated exosomes. These results were compared to those obtained from PC3 cells. Furthermore, a NTA was carried out to verify the size distribution of the isolated plasma and urinary exosomes. The results, shown in Figure 4D,E, confirmed that the number of exosomes in blood and urine in mPCa patients, PCa patients, and BPH patients progressively decreased.

Sample Detection. To demonstrate the practicality of our method in detecting exosomal miR-141 expression in biological samples, we performed total RNA extraction from exosomes derived from the plasma and urine of three patient groups, namely, BPH, PCa, and mPCa. After at least three repetitions, the results obtained from our proposed strategy showed remarkable consistency with those from qRT-PCR (Figure 4F,G), a standard miRNA detection method, effectively and

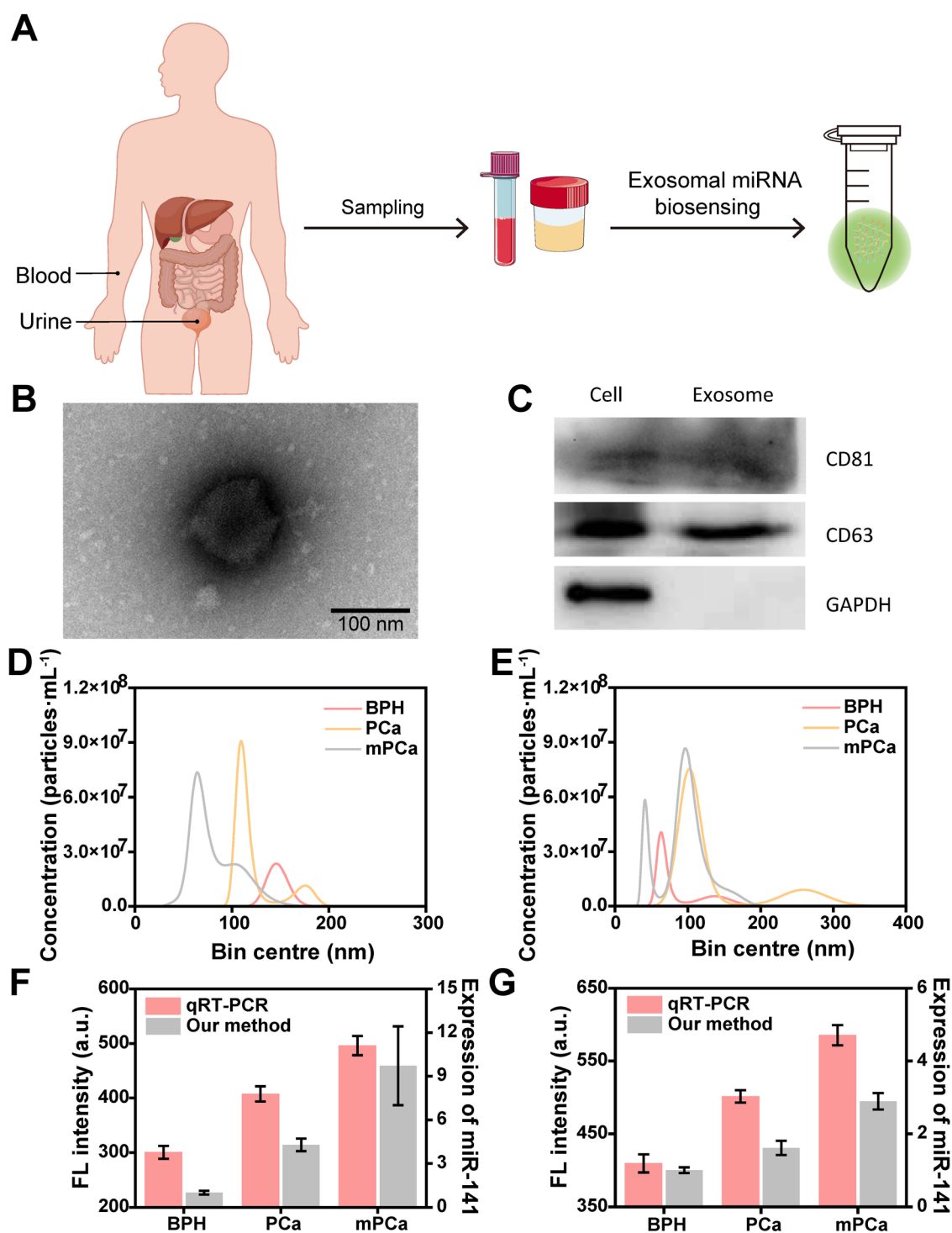


Figure 4. Exosomal characterization and quantitation of exosomal miR-141. (A) The workflow for utilizing exosomal miRNAs in our study. (B) Transmission electron microscope. (C) Western blotting. Exosomal concentrations of different cohorts in (D) urine and (E) plasma. Quantitation of exosomal miR-141 of different cohorts in (F) urine and (G) plasma by qRT-qPCR and our method. Concentrations: miR-141, 10 nM; H1, H2, H3, H4, 100 nM.

accurately distinguishing the disease status of patients. Our noninvasive liquid biopsy approach, utilizing plasma and urine samples, offers a precise and reliable diagnostic capability, making it a promising and novel tool for accurate diagnosis and treatment of PCa. This method holds significant potential to assist medical practitioners in making well-informed decisions.

CONCLUSIONS

In conclusion, we have successfully developed an enzyme-free fluorescence biosensing method for the accurate diagnosis of PCa based on dumbbell dual-hairpin triggered DNA nanonet assembly. This innovative strategy combines dumbbell dual-hairpin and DNA nanonet assembly, resulting in significantly enhanced detection sensitivity and specificity. One of the major

advantages of this approach is its simplicity, as it involves an isothermal reaction process that eliminates the need for complex protocols, expensive and perishable enzymes, and sophisticated equipment. This streamlined method not only improves accessibility but also reduces costs, making it a more practical and cost-effective option for use in clinical settings.

Furthermore, the versatility of the proposed strategy is noteworthy, as it can be easily adapted for various diseases and applications. For instance, by targeting the specific target of interest and simply modifying the fragment of complementary H1 and corresponding H2, H3, and H4, the method can be applied to diagnose nucleic-acid-related diseases, detect aptamer-based protein targets, and even enable *in vivo* imaging. This adaptability and flexibility open up a wide range of possibilities for its utilization in diverse diagnostic scenarios.

The development of this dumbbell dual-hairpin-triggered DNA nanonet assembly approach represents a significant advancement in the field of diagnostics, offering a promising and powerful tool for the accurate and efficient detection of biomarkers. Its potential applications extend beyond PCa diagnosis, presenting exciting opportunities for broader diagnostic applications in the medical field.

■ ASSOCIATED CONTENT

SI Supporting Information

The Supporting Information is available free of charge at <https://pubs.acs.org/doi/10.1021/acsomega.4c02652>.

Sequences used in this study, fluorescence profile data of the proposed method, qRT-PCR for detection of exosomal miRNA in testing clinical samples, verification of our design by an atomic force microscope, and repeatability of the prepared nanochannels (PDF)

■ AUTHOR INFORMATION

Corresponding Authors

Ming Chen – Department of Clinical Laboratory Medicine, Southwest Hospital, Third Military Medical University (Army Medical University), Chongqing 400038, P. R. China; orcid.org/0000-0003-0613-7932; Email: chming1971@126.com

Ji Zheng – Department of Urology, Urologic Surgery Center, Xinqiao Hospital, Third Military Medical University (Army Medical University), Chongqing 400037, P. R. China; School of Medicine, Chongqing University, Chongqing 400030, P. R. China; Email: jizheng023@aliyun.com

Kai Chang – Department of Clinical Laboratory Medicine, Southwest Hospital, Third Military Medical University (Army Medical University), Chongqing 400038, P. R. China; orcid.org/0000-0001-7587-3066; Email: changkai0203@tmmu.edu.cn

Authors

Yongxing Li – Department of Clinical Laboratory Medicine, Southwest Hospital, Third Military Medical University (Army Medical University), Chongqing 400038, P. R. China; Department of Urology, Urologic Surgery Center, Xinqiao Hospital, Third Military Medical University (Army Medical University), Chongqing 400037, P. R. China; School of Medicine, Chongqing University, Chongqing 400030, P. R. China

Xiaoqi Tang – Department of Clinical Laboratory Medicine, Southwest Hospital, Third Military Medical University (Army Medical University), Chongqing 400038, P. R. China

Ruijia Deng – Department of Clinical Laboratory Medicine, Southwest Hospital, Third Military Medical University (Army Medical University), Chongqing 400038, P. R. China

Liu Feng – Department of Clinical Laboratory Medicine, Southwest Hospital, Third Military Medical University (Army Medical University), Chongqing 400038, P. R. China; orcid.org/0000-0003-4926-9169

Shuang Xie – Department of Clinical Laboratory Medicine, Southwest Hospital, Third Military Medical University (Army Medical University), Chongqing 400038, P. R. China

Complete contact information is available at:

<https://pubs.acs.org/10.1021/acsomega.4c02652>

Author Contributions

Y.L. and X.T. contributed equally to this work. The manuscript was composed through the combined efforts of all authors. All authors have approved the final version of the manuscript.

Notes

The authors declare no competing financial interest.

■ ACKNOWLEDGMENTS

This work was supported by the National Natural Science Foundation of China (No. 82122042, 82372352), the Natural Science Foundation of Chongqing (No. CSTB2022NSCQ-JQX0007, CSTB2022NSCQ-MSX0862), and Chongqing Science and Health Joint Fund for Top Young and Middle-aged Talent (No. 2023GDRC007).

■ REFERENCES

- (1) Thakur, A.; Parra, D. C.; Motallebnejad, P.; Brocchi, M.; Chen, H. J. Exosomes: Small vesicles with big roles in cancer, vaccine development, and therapeutics. *Bioact. Mater.* **2022**, *10*, 281 DOI: [10.1016/j.bioactmat.2021.08.029](https://doi.org/10.1016/j.bioactmat.2021.08.029).
- (2) Yu, W.; Hurley, J.; Roberts, D.; Chakraborty, S. K.; Enderle, D.; Noerholm, M.; Breakefield, X. O.; Skog, J. K. Exosome-based liquid biopsies in cancer: opportunities and challenges. *Ann. Oncol.* **2021**, *32* (4), 466–477.
- (3) Yu, D.; Li, Y.; Wang, M.; Gu, J.; Xu, W.; Cai, H.; Fang, X.; Zhang, X. Exosomes as a new frontier of cancer liquid biopsy. *Mol. Cancer* **2022**, *21* (1), No. 56, DOI: [10.1186/s12943-022-01509-9](https://doi.org/10.1186/s12943-022-01509-9).
- (4) Gao, Z.; Pang, B.; Li, J.; Gao, N.; Fan, T.; Li, Y. Emerging Role of Exosomes in Liquid Biopsy for Monitoring Prostate Cancer Invasion and Metastasis. *Front. Cell Dev. Biol.* **2021**, *9*, No. 679527.
- (5) Krylova, S. V.; Feng, D. The Machinery of Exosomes: Biogenesis, Release, and Uptake. *Int. J. Mol. Sci.* **2023**, *24* (2), No. 1337, DOI: [10.3390/ijms24021337](https://doi.org/10.3390/ijms24021337).
- (6) Syed, S. N.; Brune, B. Exosomal and Non-Exosomal MicroRNAs: New Kids on the Block for Cancer Therapy. *Int. J. Mol. Sci.* **2022**, *23* (9), No. 4493, DOI: [10.3390/ijms23094493](https://doi.org/10.3390/ijms23094493).
- (7) Hanjani, N. A.; Esmaelizad, N.; Zanganeh, S.; Gharavi, A. T.; Heidarizadeh, P.; Radfar, M.; Omidi, F.; MacLoughlin, R.; Doroudian, M. Emerging role of exosomes as biomarkers in cancer treatment and diagnosis. *Crit. Rev. Oncol./Hematol.* **2022**, *169*, No. 103565.
- (8) Wu, Y.; Niu, D.; Deng, S.; Lei, X.; Xie, Z.; Yang, X. Tumor-derived or non-tumor-derived exosomal noncodingRNAs and signaling pathways in tumor microenvironment. *Int. Immunopharmacol.* **2022**, *106*, No. 108626.
- (9) Li, C.; Ni, Y.-Q.; Xu, H.; Xiang, Q.-Y.; Zhao, Y.; Zhan, J.-K.; He, J.-Y.; Li, S.; Liu, Y.-S. Roles and mechanisms of exosomal non-coding RNAs in human health and diseases. *Signal Transduction Targeted Ther.* **2021**, *6* (1), No. 383, DOI: [10.1038/s41392-021-00779-x](https://doi.org/10.1038/s41392-021-00779-x).

- (10) Wang, J.; Ni, J.; Beretov, J.; Thompson, J.; Graham, P.; Li, Y. Exosomal microRNAs as liquid biopsy biomarkers in prostate cancer. *Crit. Rev. Oncol./Hematol.* **2020**, *145*, No. 102860.
- (11) Naito, Y.; Yoshioka, Y.; Ochiya, T. Intercellular crosstalk between cancer cells and cancer-associated fibroblasts via extracellular vesicles. *Cancer Cell Int.* **2022**, *22* (1), No. 367, DOI: 10.1186/s12935-022-02784-8.
- (12) Baassiri, A.; Nassar, F.; Mukherji, D.; Shamseddine, A.; Nasr, R.; Temraz, S. Exosomal Non Coding RNA in LIQUID Biopsies as a Promising Biomarker for Colorectal Cancer. *Int. J. Mol. Sci.* **2020**, *21* (4), No. 1398, DOI: 10.3390/ijms21041398.
- (13) Sun, Z.; Shi, K.; Yang, S.; Liu, J.; Zhou, Q.; Wang, G.; Song, J.; Li, Z.; Zhang, Z.; Yuan, W. Effect of exosomal miRNA on cancer biology and clinical applications. *Mol. Cancer* **2018**, *17* (1), No. 147, DOI: 10.1186/s12943-018-0897-7.
- (14) Li, B.; Cao, Y.; Sun, M.; Feng, H. Expression, regulation, and function of exosome-derived miRNAs in cancer progression and therapy. *FASEB J.* **2021**, *35* (10), No. e21916.
- (15) Baldasici, O.; Pilecki, V.; Cruceriu, D.; Gavrilas, L. I.; Tudoran, O.; Balacescu, L.; Vlase, L.; Balacescu, O. Breast Cancer-Delivered Exosomal miRNA as Liquid Biopsy Biomarkers for Metastasis Prediction: A Focus on Translational Research with Clinical Applicability. *Int. J. Mol. Sci.* **2022**, *23* (16), No. 9371, DOI: 10.3390/ijms23169371.
- (16) Zhu, L.; Zhao, L.; Wang, Q.; Zhong, S.; Guo, X.; Zhu, Y.; Bao, J.; Xu, K.; Liu, S. Circulating exosomal miRNAs and cancer early diagnosis. *Clin. Transl. Oncol.* **2022**, *24* (3), 393–406.
- (17) Movahedpour, A.; Khatami, S. H.; Karami, N.; Vakili, O.; Naeli, P.; Jamali, Z.; Shabaninejad, Z.; Tazik, K.; Behrouj, H.; Ghasemi, H. Exosomal noncoding RNAs in prostate cancer. *Clin. Chim. Acta* **2022**, *537*, 127–132.
- (18) Chowdhury, S. G.; Ray, R.; Karmakar, P. Exosomal miRNAs-a diagnostic biomarker acting as a guiding light in the diagnosis of prostate cancer. *Funct. Integr. Genomics* **2023**, *23* (1), No. 23, DOI: 10.1007/s10142-022-00951-8.
- (19) Lin, B.; Jiang, J.; Jia, J.; Zhou, X. Recent Advances in Exosomal miRNA Biosensing for Liquid Biopsy. *Molecules* **2022**, *27* (21), No. 7145, DOI: 10.3390/molecules27217145.
- (20) Xu, J.; Liu, Y.; Li, Y.; Liu, Y.; Huang, K. J. Smartphone-Assisted Flexible Electrochemical Sensor Platform by a Homology DNA Nanomanager Tailored for Multiple Cancer Markers Field Inspection. *Anal. Chem.* **2023**, *95* (35), 13305–13312.
- (21) Dong, P.; Li, R.; He, S.; Zhang, Q.; Shang, J.; Jiang, Y.; Liu, X.; Wang, F. The compact integration of a cascaded HCR circuit for highly reliable cancer cell discrimination. *Chem. Sci.* **2023**, *14* (8), 2159–2167.
- (22) Han, X.; Yu, H.; Zhang, L.; Weng, Z.; Dai, L.; Wang, L.; Song, L.; Wang, Z.; Zhao, R.; Wang, L.; Wang, W.; Bai, D.; Guo, Y.; Lv, K.; Xie, G. Movable toehold for leakless self-assembly circuits. *Biosens. Bioelectron.* **2024**, *245*, No. 115823, DOI: 10.1016/j.bios.2023.115823.
- (23) Abolhasan, R.; Mehdizadeh, A.; Rashidi, M. R.; Aghebati-Maleki, L.; Yousefi, M. Application of hairpin DNA-based biosensors with various signal amplification strategies in clinical diagnosis. *Biosens. Bioelectron.* **2019**, *129*, 164–174.
- (24) Kalogianni, D. P. Nanotechnology in emerging liquid biopsy applications. *Nano Convergence* **2021**, *8* (1), No. 13, DOI: 10.1186/s40580-021-00263-w.
- (25) Hua, Y.; Ma, J.; Li, D.; Wang, R. DNA-Based Biosensors for the Biochemical Analysis: A Review. *Biosensors* **2022**, *12* (3), No. 183, DOI: 10.3390/bios12030183.
- (26) Chai, H.; Cheng, W.; Jin, D.; Miao, P. Recent Progress in DNA Hybridization Chain Reaction Strategies for Amplified Biosensing. *ACS Appl. Mater. Interfaces* **2021**, *13* (33), 38931–38946.
- (27) Xu, J.; Liu, Y.; Luo, X.; Li, Y.; Xing, Y.; Huang, K.-J. Visual self-powered platform for ultrasensitive heavy metal detection designed on graphdiyne/graphene heterojunction and DNAzyme-triggered DNA circuit strategy. *Chem. Eng. J.* **2024**, *485*, No. 150151, DOI: 10.1016/j.cej.2024.150151.
- (28) Zhang, C.; Chen, J.; Sun, R.; Huang, Z.; Luo, Z.; Zhou, C.; Wu, M.; Duan, Y.; Li, Y. The Recent Development of Hybridization Chain Reaction Strategies in Biosensors. *ACS Sens.* **2020**, *5* (10), 2977–3000.
- (29) Zeng, Z.; Zhou, R.; Sun, R.; Zhang, X.; Cheng, Z.; Chen, C.; Zhu, Q. Nonlinear hybridization chain reaction-based functional DNA nanostructure assembly for biosensing, bioimaging applications. *Biosens. Bioelectron.* **2021**, *173*, No. 112814.
- (30) Wu, J.; Lv, J.; Zheng, X.; Wu, Z. S. Hybridization chain reaction and its applications in biosensing. *Talanta* **2021**, *234*, No. 122637.
- (31) Li, H.; Wang, X.; Wei, S.; Zhao, C.; Song, X.; Xu, K.; Li, J.; Pang, B.; Wang, J. Applications of hybridization chain reaction optical detection incorporating nanomaterials: A review. *Anal. Chim. Acta* **2022**, *1190*, No. 338930.
- (32) Dirks, R. M.; Pierce, N. A. Triggered amplification by hybridization chain reaction. *Proc. Natl. Acad. Sci. U.S.A.* **2004**, *101*, 15275–15278.
- (33) Chang, C. C.; Chen, C. Y.; Chuang, T. L.; Wu, T. H.; Wei, S. C.; Liao, H.; Lin, C. W. Aptamer-based colorimetric detection of proteins using a branched DNA cascade amplification strategy and unmodified gold nanoparticles. *Biosens. Bioelectron.* **2016**, *78*, 200–205.
- (34) Cao, X.; Dong, J.; Sun, R.; Zhang, X.; Chen, C.; Zhu, Q. A DNAzyme-enhanced nonlinear hybridization chain reaction for sensitive detection of microRNA. *J. Biol. Chem.* **2023**, *299* (6), No. 104751.
- (35) Khajouei, S.; Hosseinzadeh, E.; Ravan, H.; Mohammadi, A. Binary detection of protein and nucleic acid enabled cancer diagnosis through branched hybridization chain reaction. *Anal. Chim. Acta* **2022**, *1205*, No. 339755.
- (36) Ji, P.; Han, G.; Huang, Y.; Jiang, H.; Zhou, Q.; Liu, X.; Kong, D. Ultrasensitive ratiometric detection of Pb(2+) using DNA tetrahedron-mediated hyperbranched hybridization chain reaction. *Anal. Chim. Acta* **2021**, *1147*, 170–177.
- (37) Qin, Y.; Li, D.; Yuan, R.; Xiang, Y. Netlike hybridization chain reaction assembly of DNA nanostructures enables exceptional signal amplification for sensing trace cytokines. *Nanoscale* **2019**, *11* (35), 16362–16367.
- (38) Dong, J.; Zeng, Z.; Sun, R.; Zhang, X.; Cheng, Z.; Chen, C.; Zhu, Q. Specific and sensitive detection of CircRNA based on netlike hybridization chain reaction. *Biosens. Bioelectron.* **2021**, *192*, No. 113508.
- (39) Yang, Y.; Liu, X.; Zhang, N.; Jiang, W. The dumbbell probe mediated triple cascade signal amplification strategy for sensitive and specific detection of uracil DNA glycosylase activity. *Talanta* **2021**, *234*, No. 122680.
- (40) Li, C. C.; Hu, J.; Zou, X.; Luo, X.; Zhang, C. Y. Construction of a Structure-Switchable Toehold Dumbbell Probe for Sensitive and Label-Free Measurement of MicroRNA in Cancer Cells and Tissues. *Anal. Chem.* **2022**, *94* (3), 1882–1889.
- (41) Li, B.; Xia, A.; Xie, S.; Lin, L.; Ji, Z.; Suo, T.; Zhang, X.; Huang, H. Signal-Amplified Detection of the Tumor Biomarker FEN1 Based on Cleavage-Induced Ligation of a Dumbbell DNA Probe and Rolling Circle Amplification. *Anal. Chem.* **2021**, *93* (6), 3287–3294.
- (42) Zhang, Q.; Han, Y.; Li, C. C.; Zou, X.; Ma, F.; Zhang, C. Y. Construction of a dual-functional dumbbell probe-based fluorescent biosensor for cascade amplification detection of miRNAs in lung cancer cells and tissues. *Chem. Commun.* **2022**, *58* (36), 5538–5541.
- (43) Jiang, P.; Bai, Y.; Yan, L.; Feng, P.; Huang, K.; Chen, J.; Chen, P. Nanoarchitectonics-Assisted Simultaneous Fluorescence Detection of Urinary Dual miRNAs for Noninvasive Diagnosis of Prostate Cancer. *Anal. Chem.* **2023**, *95* (19), 7676–7684.
- (44) Zhou, J.; Sun, Y.; Zhang, J.; Luo, F.; Ma, H.; Guan, M.; Feng, J.; Dong, X. Dumbbell Aptamer Sensor Based on Dual Biomarkers for Early Detection of Alzheimer's Disease. *ACS Appl. Mater. Interfaces* **2023**, *15* (13), 16394–16407.
- (45) Xu, J.; Liu, Y.; Huang, K.-J.; Wang, R.; Li, J. Cascade amplification strategy based on ultra-thin graphdiyne and CRISPR/Cas for real-time detection of tumor biomarker. *Chem. Eng. J.* **2023**, *466*, No. 143230, DOI: 10.1016/j.cej.2023.143230.

(46) Xu, J.; Liu, Y.; Huang, K. J.; Hou, Y. Y.; Sun, X.; Li, J. Real-Time Biosensor Platform Based on Novel Sandwich Graphdiyne for Ultrasensitive Detection of Tumor Marker. *Anal. Chem.* **2022**, *94* (49), 16980–16986.

(47) Li, Z.; Ma, Y. Y.; Wang, J.; Zeng, X. F.; Li, R.; Kang, W.; Hao, X. K. Exosomal microRNA-141 is upregulated in the serum of prostate cancer patients. *Oncotargets Ther.* **2016**, *9*, 139–48.

(48) Chai, S. Q.; Lv, W. Y.; He, J. H.; Li, Y. F.; Zou, H. Y.; Li, C. M.; Huang, C. Z. Highly Sensitive Detection of miR-21 through Target-Activated Catalytic Hairpin Assembly of X-Shaped DNA Nanostructures. *Anal. Chem.* **2021**, *93* (43), 14545–14551.

(49) Sun, Z.; Li, J.; Tong, Y.; Han, H.; Yang, Y.; Wang, C.; Li, H.; Du, L.; Jiang, Y. A ratiometric fluorescent biosensor based on self-fluorescent MOF and target-triggered rolling circle amplification for sensitive detection of exosome-derived miRNA. *Anal. Chim. Acta* **2022**, *1221*, No. 340136, DOI: 10.1016/j.aca.2022.340136.

(50) Wang, S.; Wang, L.; Xu, X.; Li, X.; Jiang, W. MnO₂ nanosheet-mediated ratiometric fluorescence biosensor for MicroRNA detection and imaging in living cells. *Anal. Chim. Acta* **2019**, *1063*, 152–158.

(51) Pan, M.; Liang, M.; Sun, J.; Liu, X.; Wang, F. Lighting Up Fluorescent Silver Clusters via Target-Catalyzed Hairpin Assembly for Amplified Biosensing. *Langmuir* **2018**, *34* (49), 14851–14857.

(52) Wang, Z.; Xue, Z.; Hao, X.; Miao, C.; Zhang, J.; Zheng, Y.; Zheng, Z.; Lin, X.; Weng, S. Ratiometric fluorescence sensor based on carbon dots as internal reference signal and T7 exonuclease-assisted signal amplification strategy for microRNA-21 detection. *Anal. Chim. Acta* **2020**, *1103*, 212–219.